Journal of Power Sources 196 (2011) 6055–6061

Contents lists available at ScienceDirect

Journal of Power Sources

journal homepage: www.elsevier.com/locate/jpowsour

Synthesis of silver nanoparticles on carbon papers for electrochemical catalysts

Chien-Te Hsieh*, Ching Pan, Wei-Yu Chen

Department of Chemical Engineering and Materials Science, Yuan Ze Fuel Cell Center, Yuan Ze University, Taoyuan 320, Taiwan

ARTICLE INFO

Article history:
Received 20 March 2011
Accepted 29 March 2011
Available online 5 April 2011

Keywords:
Silver nanoparticles
Electrochemical catalysts
Alkaline fuel cell
Microwave heating
Electrochemical impedance spectroscopy

ABSTRACT

This article reports two routes, microwave-assisted synthesis and thermal reduction, to deposit silver nanoparticles on oxidized carbon paper (CP) electrodes. In comparison, as-grown Ag particles, prepared by the microwave-assisted route, exhibit uniform particle size and well-dispersion over the CP substrate. Electrochemical behavior of Ag–CP electrodes is characterized by cyclic voltammetry and AC impedance spectroscopy, incorporated with equivalent circuit. Both the catalyst electrodes display redox reversibility within the potential region of 0–0.5 V vs. saturated calomel electrode (SCE) in 1 M NaOH. According to the Randles–Sevcik plot, the diffusion coefficient under voltammetric regime ranges from 9.06×10^{-10} to 3.33×10^{-10} $cm^2\ s^{-1}$. These differences of diffusion coefficient and capacitance are ascribed to the resulting Ag nanocatalysts with small particle size and no aggregation. On the basis of the results, the microwave-assisted approach for depositing nano sized Ag catalysts on CP electrodes shows the potential in application of alkaline fuel cells because of its fast synthesis, high activity, and simplicity.

1. Introduction

Recently, there has been a resurgence of interest in alkaline fuel cells (AFCs) due to usage of non-noble metal catalysts and low cost mass production, compared to other types of fuel cells such as proton exchange membrane fuel cells (PEMFCs) and direct methanol fuel cells (DMFCs) [1,2]. In an AFC, the chemical energy in fuels (e.g., hydrogen, hydrazine, or alcohol) and oxidants (oxygen) can be directly and efficiently transferred into electricity. This flexibility of fuel selection makes AFCs a promising power device for various portable electronic products [3,4]. One of the main advantages of AFCs is the replacement of Pt or Pt-based electrocatalysts with non-Pt catalysts (e.g., Au, Ni and Ag), making AFCs a potentially low cost technology compared to PEMFCs and DMFCs. It is generally recognized that the oxygen reduction reaction (ORR) in alkaline media is more facile than in acid media, reinforcing the feasibility of less expensive catalysts in place of Pt possible. Among these non-Pt catalysts, Ag nanoparticle serves as an encouraging candidate to Pt catalyst due to its high activity in alkaline solutions for ORR. It is known that silver possesses the highest electrical conductivity of any element, and is approximately 100 times less expensive than platinum [1]. Several approaches such as electroless plating [5,6], chemical reduction [3,7–9], electrochemical deposition [10], ion beam assisted deposition [11], have been developed to synthesize Ag nanostructures. However, there are few reports focused on the facile synthesis of Ag nanoparticles on carbon matrix, and their electrochemical activity in alkaline electrolyte still requires a better understanding.

To approximate practical application, carbon paper (CP), composed of microscaled carbon fibers, was chosen as support in this work. Two facile routes, microwave-assisted and chemical impregnation, were applied to deposit nano sized Ag particles on CP substrate, forming Ag–CP catalyst electrodes. Microwave heating is fast emerging as a novel processing technology for a variety of inorganic syntheses [12]. The microwave heating enables the fast transfer of microwave energy to thermal energy in polar solution. The penetration property of electromagnetic radiation is capable of inducing a uniform heating for reaction solution, thus giving size-controlled synthesis of nanoparticles. Our previous study [13] has applied a microwave-assisted method, using ethylene glycol as reducing agent, to deposit Pt nanoparticles onto carbon nanotubes. As-deposited Pt particles, with an average size of 3–5 nm, showed uniform size distribution and high electrochemical activity in acid electrolyte. In the present work, microwave deposition was proposed to grow Ag nanoparticles on CP in water. For comparison, the other method, chemical impregnation followed by thermal reduction in hydrogen atmosphere, was also used to prepare Ag particles on CP substrate. This work intends to clarify not only structural properties but also electrochemical behavior of Ag–CP catalysts in alkaline electrolyte by using cyclic voltammetry (CV) and AC impedance. The aims of this study are to shed some light on how (i) the preparation methods affects as-grown Ag structures and loading on CP, and (ii) the electrochemical activity and inner resistance of Ag–CP catalyst electrodes.

* Corresponding author. Tel.: +886 3 4638800x2577; fax: +886 3 4559373.
E-mail address: cthsieh@saturn.yzu.edu.tw (C.-T. Hsieh).

0378-7753/$ – see front matter © 2011 Elsevier B.V. All rights reserved.
doi:10.1016/j.jpowsour.2011.03.087

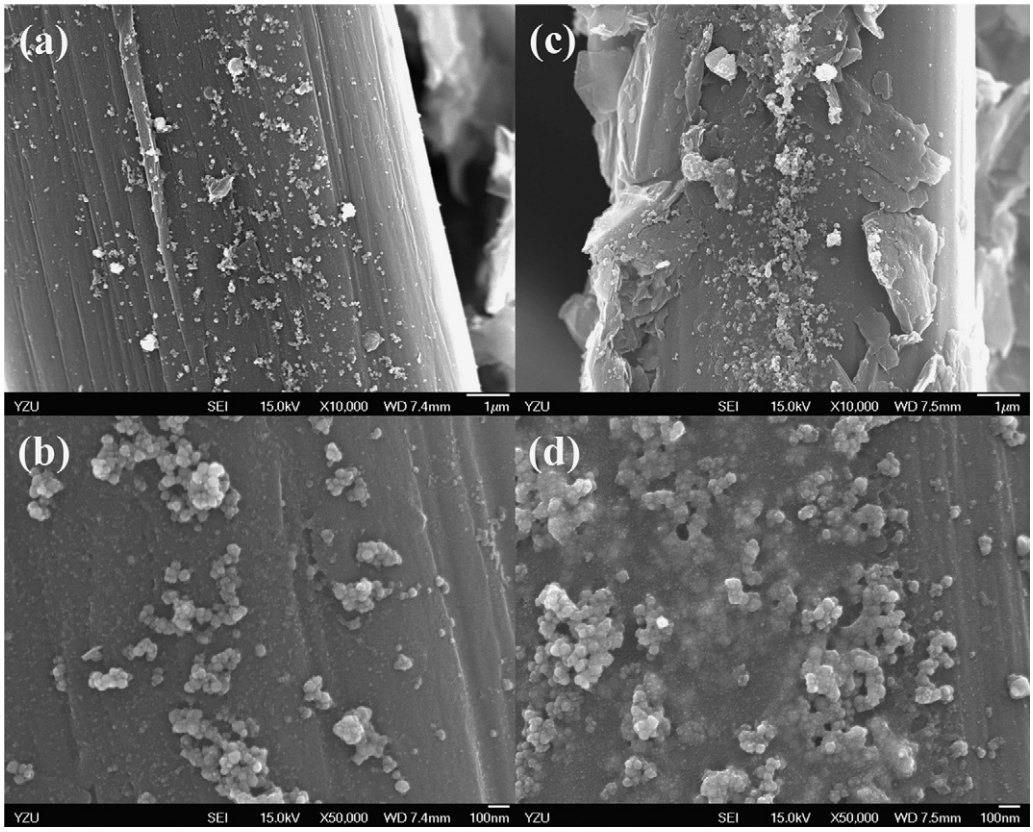

Fig. 1. FE-SEM images of as-grown silver nanoparticles over oxidized CP substrates: Ag–CP–M at (a) low and (b) high magnification, and Ag–CP–T at (c) low and (d) high magnification.

2. Experimental

The CP samples (10BA, SGL Carbon Group, Germany) used here served as carbon substrates. This type of carbon material has been extensively used as gas diffusion layer due to its high mechanical strength and porous structure. Basically, this paper, with a 400 μm thickness, consists of irregular carbon fiber that has a diameter of approximately 8–10 μm. Prior to Ag deposition, chemical oxidation was adopted by impregnating the CP sample in 1 N HNO_3 at 90 °C for 6 h. After drying, acid-oxidized CP samples with an area of 4 cm^2 were soaked in 30 ml silver nitrate solution and stirred at room temperature for 1 h. The silver-containing solution consisted of 1 ml 0.04 M $AgNO_3$, 1 ml 0.04 M KOH, and 28 ml ethylene glycol. The Ag–CP slurry was placed in a household microwave oven (Sampo, 900 W) and heated under microwave power of 720 W for 3 min. The prepared Ag–CP sample was then separated from the Ag^+ solution and subsequently dried in vacuum oven at 50 °C overnight. The Ag–CP sample was designated to Ag–CP–M catalyst.

The chemical impregnation method was to directly soak oxidized CP in 10 ml 0.5 M silver nitrate solution and 10 ml 5 wt% polyvinylpyrrolidone (PVP). Here PVP served as a stabilizer agent. To ensure adsorption equilibrium, the ionic adsorption on the CP surface took place at room temperature for 1 h. After that, the Ag-adsorbed CP sample was filtered from the ionic solution through a filtration apparatus. The treated CP was then put in a vertical furnace, having an inner diameter of 6 cm and a length of 20 cm. The furnace temperature was ramped from room temperature to 350 °C at a heating rate of 10 °C min^{-1}. A thermal reduction treatment was performed in 7 vol% H_2 atmosphere for 40 min, giving Ag–CP–T catalyst.

The structural observation of Ag CP samples was investigated by using field-emission scanning electron microscope (FE-SEM, JEOL 2010F) and high-resolution transmission electron microscope (HR-TEM, JEOL, JEM-2100). The chemical composition of as-grown Ag particles was characterized using X-ray photoelectron spectroscopy (XPS). The XP spectra were recorded with a Fison VG ESCA210 spectrometer and Mg-K_α radiation. The crystalline structure of Ag–CP samples was characterized by X-ray diffraction (XRD) with Cu-Kα radiation, using an automated X-ray diffractometer (Shimadzu Labx XRD-6000).

Three-electrode electrochemical system was used to investigate the electrochemical activity of Ag–CP samples using 1 M NaOH as the electrolyte solution. Pt wire and saturated calomel electrode (SCE) were used as counter electrode and reference electrode, respectively. Two types of Ag–CP samples, Ag–CP–M and Ag–CP–T, served as working electrodes, prepared by pressing the CP samples on stainless steel foils (as current collector). The CV measurement of the CP electrodes was made within the potential range of −1.0 to 0.5 V vs. SCE at different sweep rates of 1, 5, and 10 mV s^{-1}. The CV scans of the CP electrodes were continuously operated for more than 200 cycles to study their electrochemical durability. An electrochemical impedance spectrum analyzer (CH Instrument, Inc., CHi 608) was used to analyze the AC electrochemical impedance spectra. In this work, the potential amplitude of ac was equal to 5 mV, and the frequency was from 100 kHz to 10 mHz. All electrochemical measurements in the present work were conducted at ambient temperature.

3. Results and discussion

Fig. 1(a)–(d) shows the FE-SEM images of Ag–CP–M and Ag–CP–T composites with low and high magnifications. The CP substrate is composed of microscaled fibers with an average size of 8 μm. The white dots over the carbon fiber represent the distribution of Ag particles, showing a well dispersion. The composition of the dots has been identified as Ag nanoparticles by

electron diffraction X-ray spectroscopy. This demonstrates that both microwave-assisted and chemical impregnation routes are able to deposit Ag nanoparticles onto CP substrates. To inspect the loading of Ag catalysts, a thermogravimetric analyzer (TGA, Perkin Elmer TA7) was implemented to analyze the amount of catalysts deposited on the CP substrates. The residual weights, assigned to the weight of Ag catalysts, can be calculated to the silver loading, that is, 0.14 and 0.32 mg cm^{-2} for Ag–CP–M and Ag–CP–T, respectively. It is worth noting that the sliver loading of Ag–CP–T is twice as high as that of Ag–CP–M. This information serves as the crucial reference for designing the catalyst electrodes with high or low silver loading in further investigation.

Typical HR-TEM images with low and high magnifications for Ag–CP–M and Ag–CP–T samples are depicted in Fig. 2. As was done for sample preparation, the Ag particles were scratched and stripped from the CP matrix under an ultrasonic bath. The dark spots, assigned to Ag particles, show spherical shape in nanoscale. Uniform Ag nanoparticles obtained by microwave-assisted approach are found to have an average diameter of 20 nm. However, the Ag particles prepared by chemical impregnation, followed by thermal reduction, tend to grow uneven spheres, thus forming sphere-stacked aggregation, as observed in Fig. 2(d). It is known that surface oxides are able to occupy the defects of carbon surface [14,15]. The CPs display a low degree of graphitization (e.g., voids or broken bonds), attached with oxide groups such as carbonyl, carboxyl, and hydroxyl groups. Thus, a number of surface oxides would act as active sites for adsorption of silver ions in liquid phase. A major dissimilarity between Ag–CP–M and Ag–CP–T depends on the reduction route, that is, microwave heating and thermal reduction. The excessive thermal reduction for 40 min tends to merge Ag deposits on the CP substrate. Therefore, the aggregation formation can be ascribed to the fact that as-grown Ag sphere easily combines with neighboring spheres together at 350 °C during the reduction period, generating bulky silver islands. In comparable with microwave heating, a well-dispersion of nucleation would take place on the CP surface due to uniform reduction in liquid phase under microwave irradiation, inducing the formation of uniform Ag spheres.

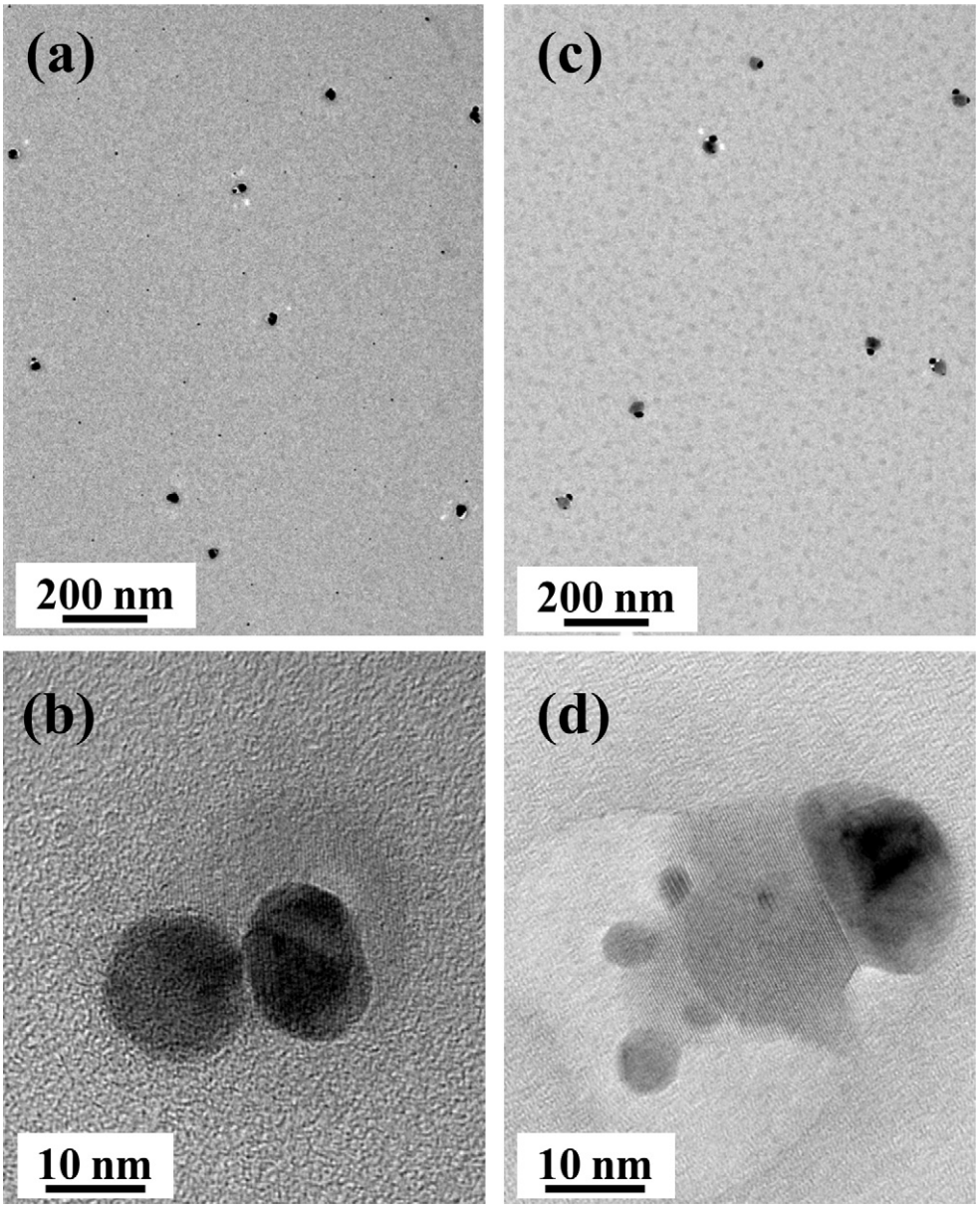

Fig. 2. HR-TEM images of as-grown silver nanoparticles: Ag–CP–M at (a) low and (b) high magnification, and Ag–CP–T at (c) low and (d) high magnification.

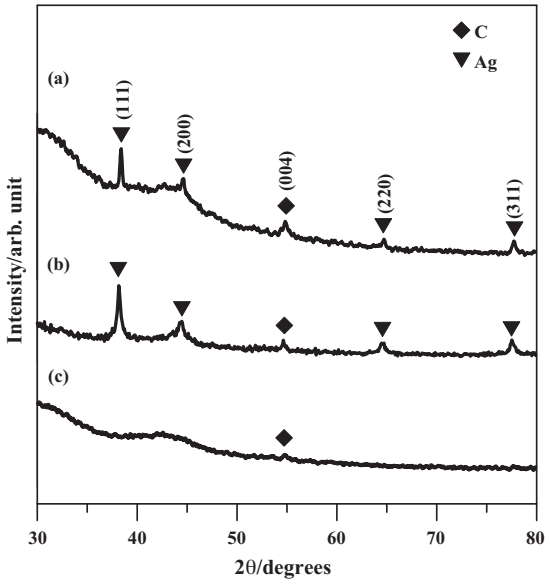

Fig. 3. Typical XRD patterns of (a) Ag–CP–M, (b) Ag–CP–T, and (c) fresh CP samples.

Fig. 3 presents the XRD patterns of different CP samples, showing the presence of Ag crystals on CP surface. The peak occurring at 26.1° and 54.8° corresponds to (0 0 2) and (0 0 4) reflections of carbon substrate. Four peaks at 2θ angles of 38.4°, 44.5°, 64.7° and 77.7° can be indexed to (1 1 1), (2 0 0), (2 2 0) and (3 1 1) reflection lines of a face-centered cubic (fcc) crystals of silver, respectively [8,16,17]. This result proves that both the synthesis routes are capable of making fcc crystal structures of Ag nanoparticles deposited on the CP surface. The average crystalline size can be calculated from the broadening of the (1 1 1) reflection by using Scherrer formula. The average grain sizes of Ag nanoparticles for Ag–CP–M and Ag–CP–T samples are 32.9 and 31.9 nm, respectively. The results are in agreement with the HR-TEM observation.

Fig. 4(a) and (b) shows XPS spectra of Ag 3d for Ag–CP–M and Ag–CP–T samples, respectively. Basically, silver is a metal that is anomalous in binding energy shifts while being oxidized, that is, the Ag 3d peaks shift to lower binding energy. The Ag 3d spectra show two distinct primary peaks for Ag $3d_{5/2}$ and Ag $3d_{3/2}$ binding energies. Both Ag $3d_{5/2}$ peaks display an asymmetric shape, which can be attributed to appearance of three components, metallic Ag, AgO, and Ag_2O, located at 368.1, 367.3 and 367.7 eV, respectively [6,18]. It can be seen that the two high intensity primary peaks represent elemental silver, showing that metallic Ag is in majority among these components. The ratios of metallic silver, determined from the integration area of Ag $3d_{5/2}$ peaks, are found to be 66.7 and 76.5% for Ag–CP–M and Ag–CP–T samples, respectively. This result indicates that both synthesis routes show fairly good ability for the reduction of metallic silver. However, it should be noticed that the period of microwave heating only takes 3 min, which is much shorter than the thermal reduction (40 min). On the basis of the above results, the microwave-assisted approach provides a facile pathway to deposit metallic Ag nanoparticles with time-saving benefit.

Typical cyclic voltammograms of Ag–CP electrodes in 1 M NaOH solution, in the potential region of −1.0 to 0.5 V vs. SCE at 10 mV s^{-1} are shown in Fig. 5. It should be noted that the redox current of Ag–CP–T approximates closely to that of Ag–CP–M electrode. As reported in literature, three anodic peaks would appear within the potential range of 0–0.5 V vs. SCE, associated with silver dissolution and formation of surface monolayer of $Ag(OH)_2^-$ (1st peak), formation of bulk phases of Ag_2O (2nd peak) and AgO (3rd peak) [3,19–21]. The reaction for the first anodic peak, related to electrodissolution of Ag to $Ag(OH)_2{}^-{}_{ads}$ through adsorption of OH^- and desorption and diffusion of soluble $Ag(OH)_2^-$, can be expressed as [21]:

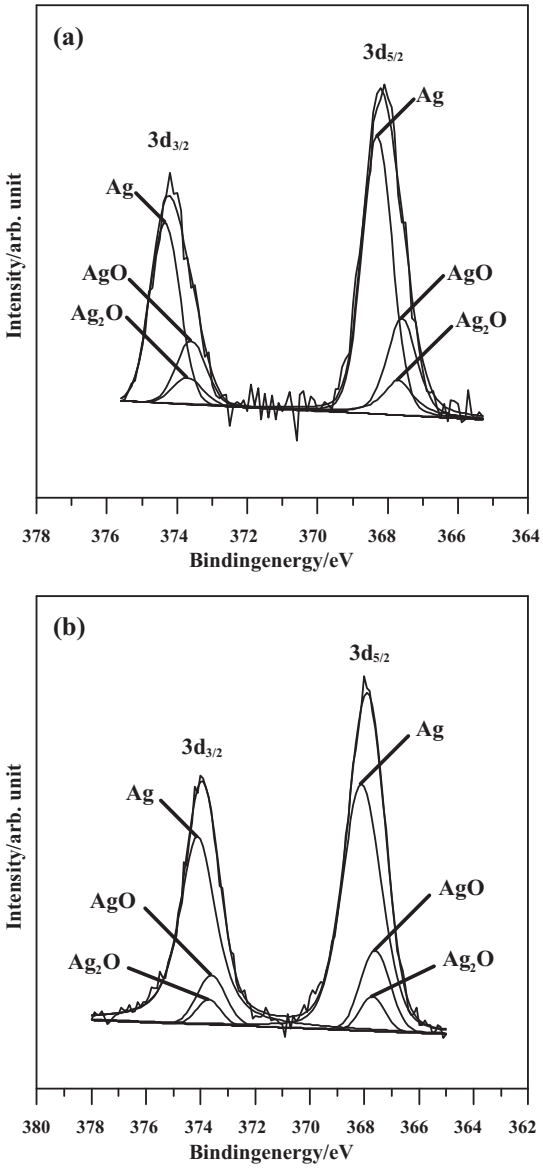

Fig. 4. XPS spectra of Ag 3d peak for (a) Ag–CP–M, and (b) Ag–CP–T samples, deconvoluted by using a symmetric multiple Gaussian function.

$$Ag + 2OH^-{}_{ads} \leftrightarrow Ag(OH)_2{}^-{}_{ads} + e^- \quad (R1)$$

$$Ag(OH)_2{}^-{}_{ads} \leftrightarrow Ag(OH)_2{}^-{}_{aq} \quad (R2)$$

However, the peak intensity seems to be imperceptible, implying that less dissolution of metallic silver occurs on the carbon surface.

The second anodic peak can be ascribed to the thickening of a completed basal monolayer, that is, the electroformation of a multilayer of Ag_2O. The thickening process occurs through nucleation and growth mechanisms according to [20,21]:

$$2Ag + 2OH^- \leftrightarrow Ag_2O + H_2O + 2e^- \quad (R3)$$

The third anodic peak originates from the electrooxidation of Ag_2O and the formation of AgO according to the overall chemical reaction [21]:

$$Ag_2O + 2OH^- \leftrightarrow 2AgO + H_2O + 2e^- \quad (R4)$$

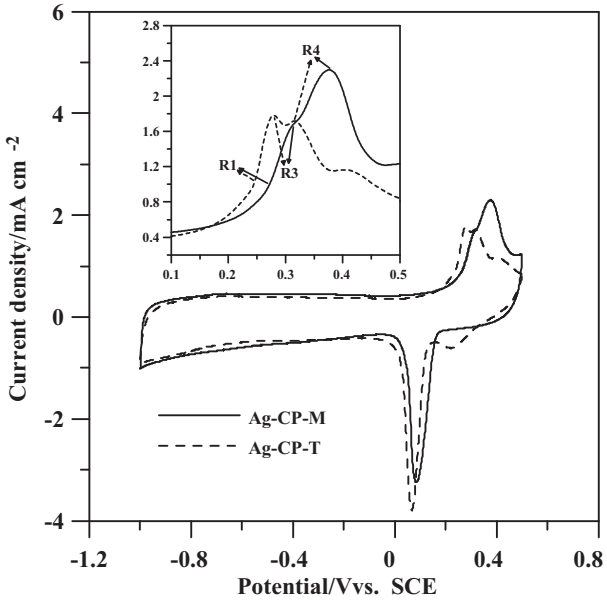

Fig. 5. Typical CV profiles for Ag–CP–M and Ag–CP–T electrodes at 10 mV s^{-1}.

Additionally, a direct electrooxidation of Ag to AgO may occur with the potential range of the third peak, which can be expressed as [21]:

$$Ag + 2OH^- \leftrightarrow AgO + H_2O + 2e^- \quad (R5)$$

In the other hand, two typical cathodic peaks take place within the potential region. The first one is attributed to the electroreduction of AgO to Ag_2O according to [21]:

$$2AgO + H_2O + 2e^- \leftrightarrow Ag_2O + 2OH^- \quad (R6)$$

Accordingly, this peak is conjugated to the third anodic peak, for example (R4). After that, the more negative cathodic peak is ascribed to the electroreduction of Ag(I) oxygen species [21].

As observed in Fig. 5, both Ag–CP electrodes exhibit very small first, and obvious second and third anodic peaks in the anodic scan. In the cathodic scan, there are two apparent peaks for both Ag–CP electrodes, showing the reversibility of redox reactions on the surface of silver catalysts. Fig. 6(a) and (d) shows the cycle voltammograms of Ag–CP electrodes at different sweep rates of 1, 5, and 10 mV s^{-1}. The redox peaks are found to show a position shift at a high sweep rate, reflecting that diffusion is the rate-determining step. For a diffusion-controlled process under potentiodynamic conditions, diffusion coefficients (D) can be calculated through Randles–Sevcik equation [22]:

$$i_p = (2.69 \times 10^5) n^{3/2} A D^{1/2} C * v^{1/2} \quad (1)$$

where i_p is the anodic peak current (A), n is the number of electrons produced in oxidation process, A is the geometric area of electrode (cm^2), C^* is the bulk concentration of electroactive species (mol cm^{-3}), and v is the sweep rate (V s^{-1}). Fig. 7 shows the linear plots of i_p vs. ($v^{1/2}$) for Ag–CP–M and Ag–CP–T electrodes, respectively. The linear plots of both catalyst electrodes with high correlation factors ($r^2 > 0.990$) demonstrate the diffusion-controlled process [23]. The D values, determined from the slopes of the plots, were found to be 9.06×10^{-10} (Ag–CP–M) and 3.33×10^{-10} cm^2 s^{-1} (Ag–CP–T). On the basis of the result, the Ag particles, prepared by the microwave heating, display higher diffusion coefficient than that by thermal reduction, that is, the promotion of D values: ~3 times, compared with Ag–CP–T electrode. This difference can be supported by the reasonable explanations

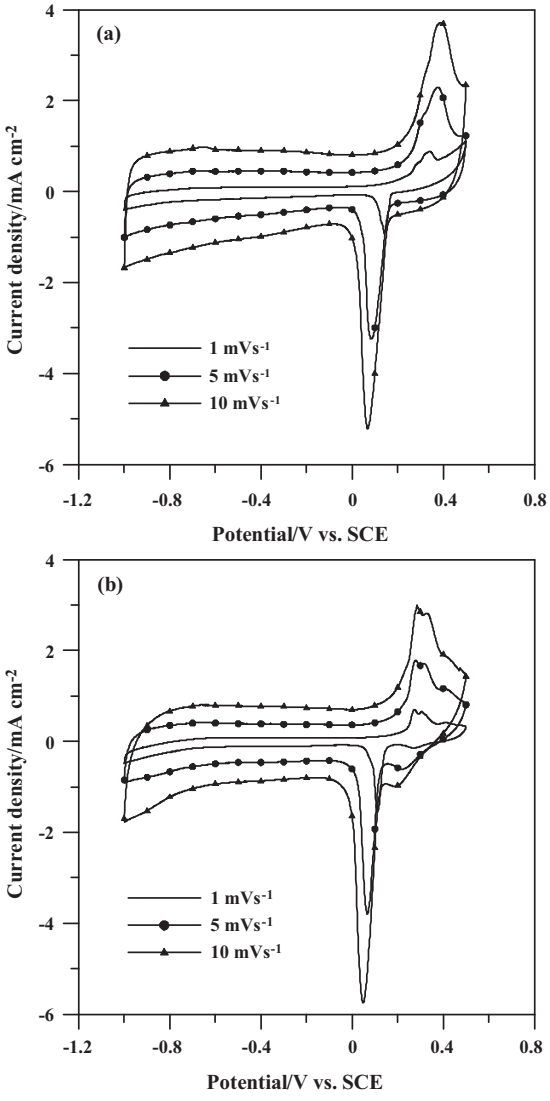

Fig. 6. Typical CV profiles for (a) Ag–CP–M and (b) Ag–CP–T electrodes at different sweep rates of 1, 5, and 10 mV s^{-1}.

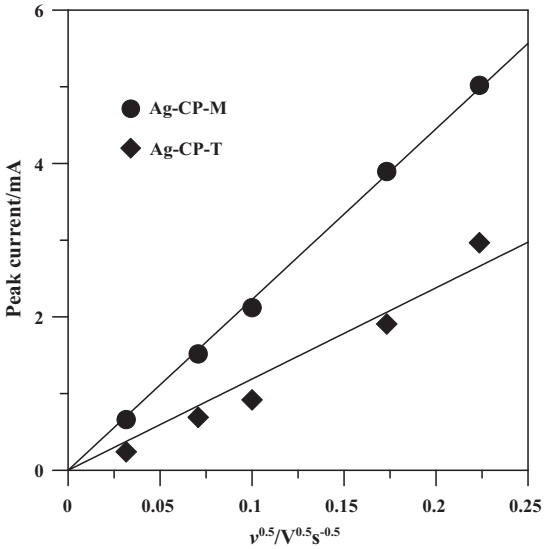

Fig. 7. Randles–Sevcik plots of different Ag–CP electrodes.

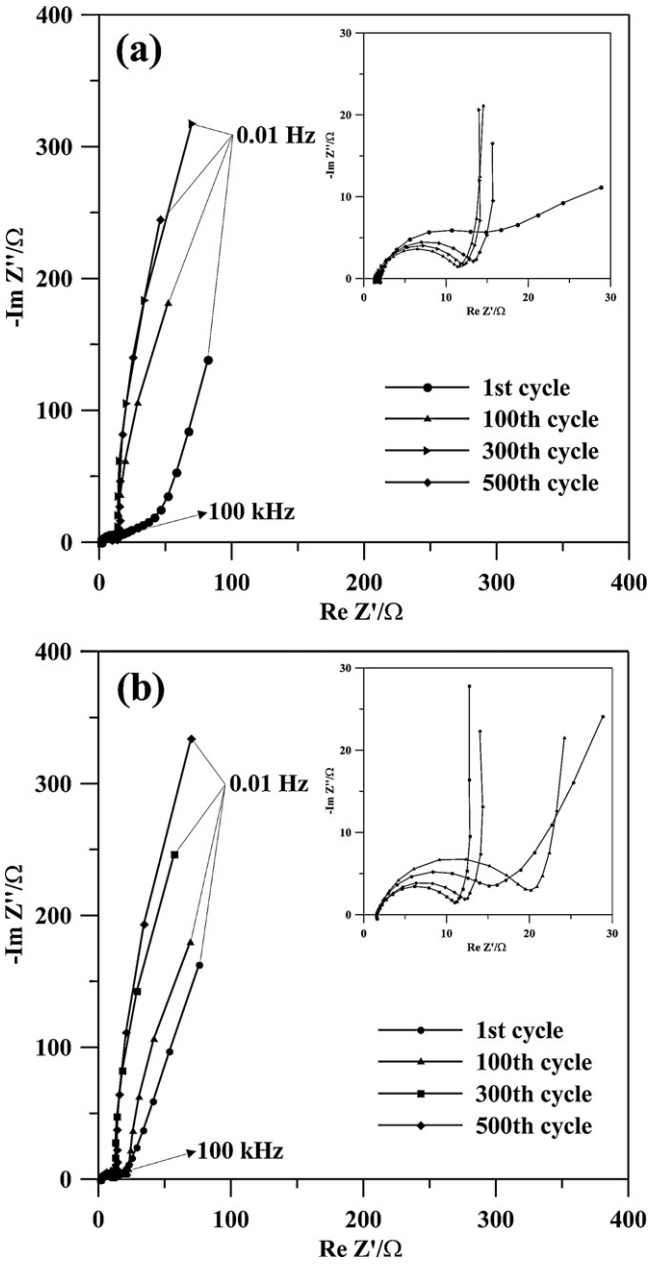

Fig. 8. Nyquist plots of different Ag–CP electrodes for (a) Ag–CP–M and (b) Ag–CP–T.

that as-grown silver in Ag–CP–M electrode possesses well dispersion, facilitating the diffusion of ions in the electrode.

The AC impedance spectroscopy was further applied to analyze the electrochemical behavior of the Ag–CP electrodes. Fig. 8 shows the Nyquist plots of both electrodes, presenting a similar profile of impedance spectra. Basically, the impedance spectra for both Ag–CP electrodes can be divided into three parts: (i) an intersection in the real axis in high-frequency region, (ii) a single depressed semicircle in the frequency region between 100 kHz and 1 Hz, and (iii) an almost-vertical line with decreasing frequency. The almost-vertical lines at low frequencies can be assigned to the capacitive response of the carbon electrodes [24,25].

An equivalent circuit was proposed to characterize the electrochemical behavior of the Ag–CP electrodes. The circuit elements consist of the bulk solution resistance, R_S; the double-layer capacitance, C_{dl}; the Faradaic resistance, R_F, corresponding to the reciprocal of the potential-dependent charge transfer rate in redox reactions; a pseudocapacitance, C_p, associated with the potential

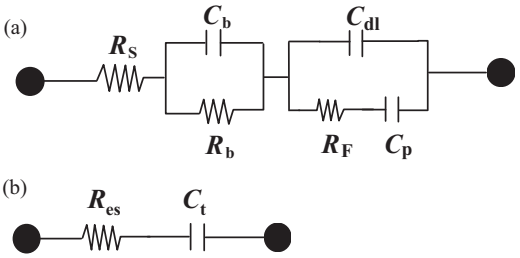

Fig. 9. Proposed equivalent circuits for Ag–CP electrodes within (a) high and (b) low frequencies.

Table 1
Components and related parameters of the equivalent circuits (Fig. 9) for the Ag–CP electrodes in 1 M NaOH (deviation for each component <9.8%).

Electrode	R_s (Ω)	R_c (Ω)	C_b (μF cm^{-2})	R_F (Ω)	$C_{dl} \pm C_p$ (F g^{-1})
Ag–CP–M	1.69	11.5	3.50	2.23	250
Ag–CP–T	1.68	10.2	3.85	2.33	177

dependence of redox-site concentration; and C_b and R_b due to the impedance between the catalyst composites and the backing plate for the electrical connection. The combination of the circuit elements is proposed and shown in Fig. 9(a). Accordingly, the overall impedance, Z, of the equivalent circuit can be expressed as [13,14,25]:

$$Z = R_S + \frac{R_b}{j\omega R_b C_b + 1} + \frac{1}{j\omega C_{dl} + \left(j\omega C_p/(j\omega R_F C_p + 1)\right)} \quad (2)$$

Basically, Eq. (2) can be divided into two limiting cases: low- and high-frequency regions. At sufficiently high frequencies, Eq. (2) corresponds to a locus showing the solution, the electrical connection resistance, and the charge transfer resistance, that is, R_S, R_b, and R_F. The overall resistance determined is the so-called equivalent serial resistance ($R_{es} = R_S + R_b + R_F$), which is composed of bulk solution resistance, connection resistance, and charge transfer resistance [26]. As shown in Fig. 9(b), the impedance in low-frequency region suggests the pure capacitive behavior [24], where the overall capacitance ($C_t = C_{dl} + C_p$), of the electrodes can be estimated.

By using Z-view computer software, the fitting parameters for both electrodes are summarized in Table 1. This table clearly shows that both the R_S values are found to be small (~1.68 Ω), showing little variation with both electrodes. The presence of R_b values originates from the connection of conductive materials (i.e., metallic Ag and CP) to the current collector (i.e., stainless foil). The R_b value of Ag–CP–M electrode shows a slight increase compared with Ag–CP–T electrode, that is, 10.2 and 11.5 Ω for Ag–CP–T and Ag–CP–M electrode, respectively. This result is presumably due to low Ag density on Ag–CP–M electrode. The R_{es} values for Ag–CP–M and Ag–CP–T electrodes are estimated to be 15.42 Ω and 14.21 Ω, respectively. It is worth noting that the R_b value can account for a major proportion of the equivalent series resistance, whereas the value of R_F plays a minor role in the R_{es} value for both electrodes.

As observed from Table 1, both C_b values can be insignificantly small compared to the overall capacitance. The overall charge transfer ($C_{dl} + C_p$) obtained from the impedance analysis indicates that Ag–CP–M electrode exhibits an electrochemical activity higher than Ag–CP–T electrode. Since pure CP electrodes are expected to have an identical C_{dl} value, the pseudocapacitance (C_p) thus contributes to the major portion in improving the overall capacitance. This capacitance, contributed from charge transfer reaction, is analogous to the electrochemical activity of silver catalysts in alkali electrolyte. On the basis of the above results, as-grown Ag catalysts, prepared by microwave heating, offer the better redox activity due to the effects of particle size and no aggregation. Accordingly, the

microwave-assisted route shows a commercial feasibility to rapidly synthesize Ag nanoparticles with high electrochemical activity, inducing the potential application for AFCs.

4. Conclusions

The results presented in this work unambiguously provide a facile route to synthesize nano sized Ag particles by using microwave-assisted and thermal reduction approaches. Both two routes enabled the deposition of crystalline Ag particles onto the oxidized CP surface. Metallic silver nanoparticles by microwave heating were found to have a narrow size distribution, compared to thermal reduction. The CV analysis indicated that (i) both silver catalysts possess the redox reversibility in alkali electrolyte and (ii) the diffusion coefficients under voltammetric regime are 9.06×10^{-10} (Ag–CP–M) and 3.33×10^{-10} $cm^2\ s^{-1}$ (Ag–CP–T). The AC impedance spectroscopy incorporated with analysis of equivalent circuit showed that Ag–CP–M catalyst exhibits higher electrochemical activity than Ag–CP–T. This increase of capacitance can be attributed to as-grown Ag with small particle size and no aggregation, leading to a great activity in the redox reaction. On the basis of the results, the microwave-assisted route for depositing nano sized Ag catalysts on CP electrodes delivers the feasibility for AFCs application due to its fast synthesis, high activity, and simplicity.

Acknowledgments

The authors are very grateful for the financial support from the National Science Council of the Republic of China under the contracts NSC 98-2120-M-155-001 and NSC 99-2221-E-155-078.

References

[1] F. Bidault, A. Kucernak, J. Power Sources 195 (2010) 1023–1032.
[2] E. Antolini, E.R. Gonzalez, J. Power Sources 195 (2010) 3431–3450.
[3] J. Guo, A. Hsu, D. Chu, R. Chen, J. Phys. Chem. C 114 (2010) 4324–4330.
[4] F. Bidault, D.J.L. Brett, P.H. Middleton, N.P. Brandon, J. Power Sources 187 (2009) 39–48.
[5] C.S. Li, B.S. Wang, Y.J. Qiao, W.Z. Lu, J. Liang, Int. J. Miner. Metall. Mater. 16 (2009) 598–602.
[6] M.A. Kostowskyj, D.W. Kirk, S.J. Thorpe, Int. J. Hydrogen Energy 35 (2010) 5666–5672.
[7] B. He, J.J. Tan, K.Y. Liew, H. Liu, J. Mol. Catal. A: Chem. 221 (2004) 121–126.
[8] C. Tan, F. Wang, J.J. Liu, Y.B. Zhao, J.J. Wang, L.H. Zhang, K.C. Park, M. Endo, Mater. Lett. 63 (2009) 969–971.
[9] L. Demarconnay, C. Coutanceau, J.M. Léger, Electrochim. Acta 49 (2004) 4513–4521.
[10] Z. Tang, S. Liu, S. Dong, E. Wang, J. Electroanal. Chem. 502 (2001) 146–151.
[11] T. Liu, H.Q. Tang, X.M. Cai, J. Zhao, D.J. Li, R. Li, X.L. Sun, Nucl. Instrum. Methods Phys. Res. B 264 (2007) 282–286.
[12] H. Yin, T. Yamamoto, Y. Wada, S. Yanagida, Mater. Chem. Phys. 83 (2004) 66–70.
[13] C.T. Hsieh, W.M. Hung, W.Y. Chen, Int. J. Hydrogen Energy 35 (2010) 8425–8432.
[14] C.T. Hsieh, W.Y. Chen, Y.S. Chen, Electrochim. Acta 55 (2010) 5294–5300.
[15] K. Kinoshita, Carbon: Electrochemical and Physicochemical Properties, John & Wiley, New York, 1987.
[16] K. Ni, L. Chen, G. Lu, Electrochem. Commun. 10 (2008) 1027–1030.
[17] Y. Gao, N. Munroe, X. Kong, K. Jones, J. Power Sources 189 (2009) 935–942.
[18] E. Tomaszewicz, M. Kurzawa, J. Mater. Sci. 39 (2004) 2183–2185.
[19] A.E. Sanli, İ. Kayacan, B.Z. Uysal, M.L. Aksu, J. Power Sources 195 (2010) 2604–2607.
[20] L. Majari-Kasmaee, F. Gobal, J. Power Sources 195 (2010) 165–169.
[21] S.S.A. El Rehim, H.H. Hassan, M.A.M. Ibrahim, M.A. Amin, Monatsh. Chem. 129 (1998) 1103–1117.
[22] J.E.B. Randles, Trans. Faraday Soc. 44 (1948) 327–338.
[23] G.W. Yang, G.Y. Gao, C. Wang, C.L. Xu, H.L. Li, Carbon 46 (2008) 747–752.
[24] B.E. Conway, Electrochemical Supercapacitors: Scientific Fundamentals and Technological Applications, Klumer Academic/Plenum Publishers, 1999.
[25] J.N. Nian, H. Teng, J. Phys. Chem. B 109 (2005) 10279–10284.
[26] S. Koh, J. Leisch, M.F. Toney, P. Strasser, J. Phys. Chem. C 111 (2007) 3744–3752.